Sun *et al. Cancer Cell International* (2025) 25:11
https://doi.org/10.1186/s12935-025-03636-x

Cancer Cell International

RESEARCH Open Access

Deapioplatycodin D inhibits glioblastoma cell proliferation by inducing BNIP3L-mediated incomplete mitophagy

Yu Sun[1,2], Guangze Zhu[3], Renshuang Zhao[4], Yaru Li[4], Hongyang Li[1], Yunyun Liu[3], Ningyi Jin[3,5], Xiao Li[3,5*], Yiquan Li[3*] and Tiemei Liu[1,6*]

Abstract

Deapioplatycodin D (DPD) is a triterpenoid saponin natural compound isolated from the Chinese herb *Platycodon grandiflorum* that has antiviral and antitumor properties. This study aimed to investigate the effects of DPD on glioblastoma (GBM) cells and to determine its intrinsic mechanism of action. Using a CCK8 assay, it was found that DPD significantly inhibited the growth of GBM cells. DPD-treated GBM cells contained swollen and degenerated mitochondria with empty vesicular bilayer membrane-like autophagic vesicle structures in the periphery of the mitochondria under transmission electron microscopy. DPD activated autophagy in GBM cells and induced a blockage of autophagic flux in the late stage. Transcriptomics identified differences in mitophagy-related genes, and analysis of the levels of the corresponding proteins indicated that mitophagy in GBM cells was induced mainly through BNIP3L. Increased expression of BNIP3L disrupts the Bcl-2-Beclin-1 complex, thereby releasing Beclin-1 and activating autophagy. Autophagy was inhibited after silencing of BNIP3L and overexpression of Bcl-2 in GBM cells, and the growth inhibitory effect of DPD was significantly reduced. This result demonstrated that DPD induces mitophagy in GBM cells through BNIP3L. Finally, activation of incomplete mitophagy in GBM cells by DPD through BNIP3L in vivo was demonstrated by establishing a mouse subcutaneous xenograft tumor model. In this study, in vitro and in vivo experiments established that DPD inhibited GBM cell growth by inducing BNIP3L-mediated incomplete mitophagy, which provides an experimental basis for studying new treatments of GBM.

Keywords Deapioplatycodin D, BNIP3L, Mitophagy, Glioblastoma

Introduction

Glioblastoma (GBM) is the most aggressive malignant primary brain tumor [1]. Even with the current standard of care, which includes surgical resection and subsequent temozolomide chemotherapy combined with radiotherapy, prognosis is still abysmal [2], with a median survival of approximately 15 months. The sensitivity of GBM to chemotherapy is limited by intrinsic resistance to apoptotic cell death. Temozolomide is a chemotherapeutic alkylating agent, but its clinical utility in GBM is limited by chemoresistance [3]. There is an urgent need to develop other therapeutic agents for GBM.

*Correspondence:
Xiao Li
lixiao06@mails.jlu.edu.cn
Yiquan Li
liyq01@ccucm.edu.cn
Tiemei Liu
ltm@jlu.edu.cn

Full list of author information is available at the end of the article

Graphical Abstract

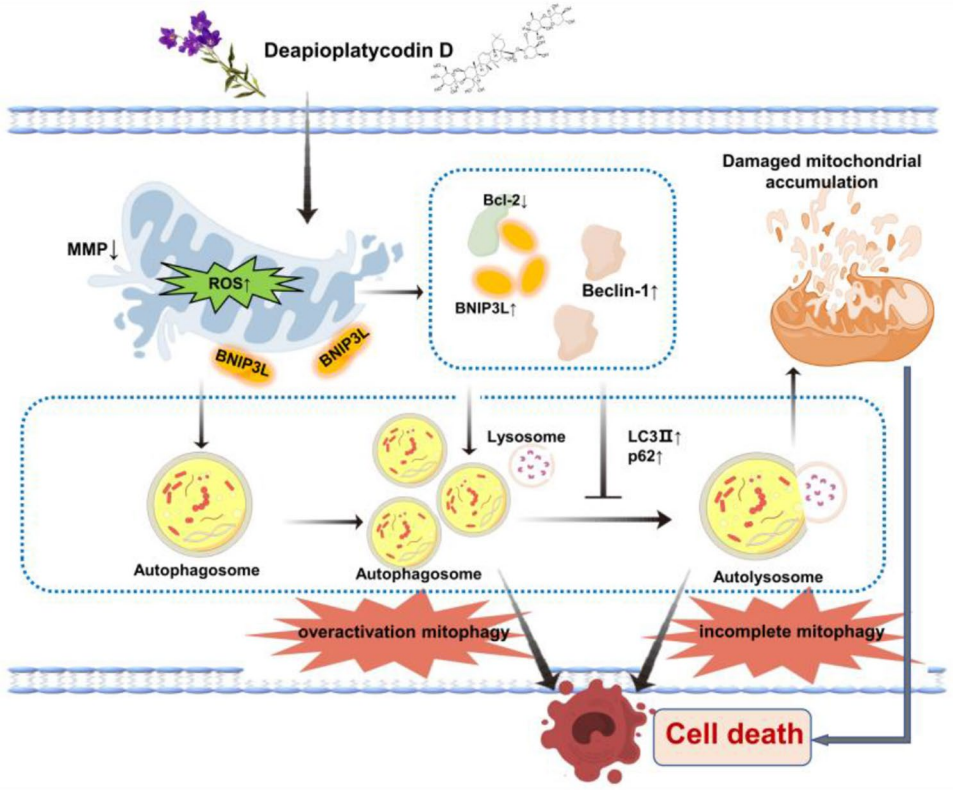

Autophagy is a conserved self-digestion system and a vital recycling mechanism for damaged cellular components [4]. Damaged lipids, proteins, and organelles are encapsulated in double-membrane vesicles (autophagosomes) and translocated to the lysosome for degradation and recycling. Cancer cells are more dependent on autophagy for survival than normal cells [5].

Mitophagy, a selective form of autophagy that targets mitochondria, has a dual role in cancer [6, 7]. It can either support tumor cell survival or promote tumor cell death, and manipulation of mitophagy has been explored as a therapeutic target for cancer. BNIP3L/NIX is a critical mitophagy receptor that responds to hypoxic conditions and induces mitophagy-mediated growth inhibition in several types of tumor. Studies have shown that p53-induced expression of BNIP3L exhibits tumor suppressor activity, and its knockdown promotes tumor growth in a xenograft model [8]. The testis antigen FATE1 maintains Ewing sarcoma cell survival by attenuating the accumulation of BNIP3L [9], suggesting that BNIP3L induces cell death. It has been shown that induction of autophagic cell death in glioma cells by AT 101, a natural compound from cotton seeds, required BNIP3L [10]. It has also been demonstrated that BNIP3L mediates mitophagy in hypoxic regions of glioblastomas [11]. BNIP3L is overexpressed in cells encapsulated in hypoxic areas of necrosis, and it scavenges reactive oxygen species (ROS) that damage mitochondria through the HIF/mTOR/RHEB pathway to maintain cancer stem cell survival. These results suggest that BNIP3L also plays a dual role in different types and stages of cancer progression and that the BNIP3L-mediated mitochondrial phagocytosis pathway may be a critical therapeutic target for tumors, including glioblastoma.

Saponins are natural chemicals with high efficacy and low toxicity that have shown good anticancer activity. Deapioplatycodin D (DPD) is a triterpenoid saponin isolated from the herb *Platycodon grandiflorum* that has a variety of biological activities [12]. Currently, the most widely researched Platycodonopsis saponin globally is platycodin D, which has exhibited significant inhibitory effects on different cancer cell lines, such as HepG-2 hepatocellular carcinoma cells [13], MCF-7 breast cancer cells [14], PC-3 prostate cancer cells [15], and GBM cells [16, 17]. However, DPD, a novel Platycodonopsis saponin analog, has been less studied in the antitumor field, and its effects on GBM and its mechanism of action have not yet been elucidated.

Materials and methods

Reagents

Deapioplatycodin D (cat. HY-N0588, purity ≥ 99.0%), temozolomide (TMZ, cat. HY-17364), 3-methyladenine (3-MA, cat. HY-19312), and bafilomycin A1 (BafA1, cat. HY-100558) were purchased from MedChemExpress (Shanghai, China). Primary antibodies against BNIP3L (cat. 12396-S), Bcl-2 (cat. 15071 S), SQSTM1/p62 (cat. 23214 S), TOM20 (cat. 42406 S), caspase-3 (cat. 14220T), cleaved PARP (cat. 5625T) and GAPDH (cat. 2118 S) were purchased from Cell Signaling Technology (Shanghai, China); other primary antibodies against Beclin-1 (cat. 11306-1-AP), LC3 (cat. 14600-1-AP), actin (cat. 20536-1-AP) and Ki67 (cat. 27309-1-AP) were purchased from Proteintech (Wuhan, China). Horseradish peroxidase-labeled goat anti-rabbit IgG (H + L, cat. A0208) and horseradish peroxidase-labeled goat anti-mouse IgG (H + L, cat. A0216) were purchased from Beyotime Biotechnology (Shanghai, China). JC-1 mitochondrial membrane potential (MMP) detection kit (JC-1, C2006), CCK8 (cat. C0039), reactive oxygen species (ROS) assay kit (DCFH-DA, S0033S) and mitophagy inhibitor Mdivi-1 (cat. SC8028). were purchased from Beyotime Biotechnology.

Cells and animals

Human glioblastoma cell lines U87MG (cat: BNCC338150), U251MG (cat: BNCC100123), and LN229MG (cat: BNCC341218) were purchased from BNCC Cell Bank (China). All GBM cell lines were supplied with STR (Short Tandem Repeat) identification reports at purchase. STR genotype test results suggested a perfect match with ExPASy cell banks U87MG (CVCL-0022) and U251MG (CVCL-0021), EV value = 1.00, and LN229MG (cell number: CVCL-0393) was an essential match with EV value = 0.96. All glioblastoma cell lines were cultured in 500 mL Dulbecco's modified Eagle medium (DMEM, Hyclone, USA) supplemented with 10% fetal bovine serum (Gibco, Australia), and 100 U/mL penicillin/0.1 mg/mL streptomycin double antibiotic (Hyclone, USA) in a humidified incubator containing 5% CO_2 humidification at 37 °C. Female BALB/c nude mice (4–5 weeks old) were purchased from GENET-MED Biotechnology Ltd.

Plasmid transfection, RNA interference, and lentivirus infection

U87MG and LN229MG cells were inoculated at 3×10^5/well in a 6-well cell culture plate. The cell density reached about 70% on the second day. The old culture medium was discarded and replaced with double-antibody-free medium, and 40 nM si-BNIP3L (RiboBio, China, SIGS0005709-4) was added to each well, followed by DPD. Negative control wells were also set up, and the cells were subjected to subsequent experiments 48 h after administration. Overexpression plasmids (pcDNA3.1(+)-Flag-Bcl-2, PPL0037-2d) were purchased from Public Protein/Plasmid Library (China) and, again using 6-well cell culture plates, 2 μg per well was mixed with the same volume of transfection reagent (Invigentech, Shanghai, China) and added to double-antibody-free medium after 15 min for subsequent experiments. U87MG and LN229MG cells, at a density of about 1×10^5 cells/well, were placed in a 12-well plate with slides and incubated for 24 h. On the second day, the cell density reached about 50%, and the cells were infected with lentivirus expressing Ad-GFP-LC3B or Ad-mCherry-GFP-LC3B for 24–36 h. After checking cell growth status and that reasonable fluorescence was observed, DPD was added and changes of fluorescence subsequently determined under a confocal electron microscope.

Cell viability assay

U87MG and LN229MG cells were cultured in 96-well plates at 8×10^3 cells/well. After 48 h of drug treatment, CCK8 solution (10 μL) was added to each well and the plates kept in the dark at 37 °C for 2 h. The optical density of each well was measured at 450 nm using an enzyme marker (Tecan, Austria) to determine cell viability.

Transmission electron microscopy (TEM)

LN229MG cells were cultured in a 6-well plate and treated with DMEM or DPD for the duration of the experiment. After collection and washing, the cells were centrifuged and the culture medium discarded. The cells were then treated with 2.5% glutaraldehyde electron microscopy fixative (Biosharp, China, BL911A) at 4 °C for 4 h. The cells were rinsed three times with 0.1 M phosphate buffered saline (PBS, pH 7.4) for 15 min each time, followed by sequential application of 50%, 70%, 80%, 90%, 95%, 100%, and 100% alcohol dehydration for 15 min each time. The cells were then embedded in SPI-Pon 812 epoxy resin (SPI, 90529-77-4). Sections were double-stained with uranium-lead (2% saturated aqueous solution of uranium acetate, lead citrate, 15 min each) and dried overnight at room temperature. Cells were observed using a transmission electron microscope (Nihon Electronics, Japan, JEM-1400Flash).

Apoptosis detection

DPD-treated GBM cells were collected, centrifuged, washed and then suspended in 1X binding buffer. The cells were sequentially stained with 5 μL of Annexin V-FITC and 5 μL of propidium iodide (PI) with protection from light (Annexin V/PI Detection Kit, B.D., USA, BD 556547). Apoptosis was determined using a FACS Calibur flow cytometer (B.D. C6 Plus, USA).

Transcriptome sequencing

LN229MG cells treated with 0 or 30 μM DPD were collected, washed with ice-cold PBS, snap-frozen in liquid nitrogen, and stored at – 80 °C until analysis. Nucleic acid extraction was accomplished using TRIzol (TIANGEN, DP424), and the concentration of the extracted nucleic acids was checked using a Nanodrop 2000 (Thermo Fisher Scientific, USA), LabChip GX (PerkinElmer, USA) and Agilent 2100 (Agilent, USA) for nucleic acid integrity testing. After library construction (VAHTS Universal V6 RNA-seq Library Prep Kit for Illumina, Vazyme Biotech Co., Ltd., Nanjing, China, No. NR604-02) and purification (VAHTS DNA Clean Beads, Vazyme Biotech Co., Ltd. Nanjing, China, No. N411-03), the constructed libraries were sequenced using an Illumina NovaSeq 6000. Fold change ≥ 1.5 and P-value < 0.05 were used as the criteria for differential gene screening.

Western blot

U87MG and LN229MG cells treated with DPD and different reagents were collected for protein extraction using a total protein extraction kit (Invent, USA, SD-001/SN-002). Proteins were quantified with a BCA kit (Beyotime, Shanghai, China, P0011). Protein from each sample (30 μg) was then separated by 12.5% SDS-PAGE (YaMei, Shanghai, China) and transferred to nitrocellulose (NC) membrane (Cyiva, China, 10600002). The NC membrane was blocked with TBST containing 5% skimmed milk for 2 h at room temperature, and then incubated with the primary antibody on a low-speed shaker at 4 °C overnight. The NC membrane was rinsed three times with TBST (10 min each time) and then secondary antibody was added and incubated on a low-speed shaker for 1 h. The membrane was rinsed three times (10 min each time) with TBST and the abundance of target protein was detected using an ECL colorimetric kit (Thermo Fisher Scientific, USA).

Immunofluorescence

U87MG and LN229MG cells treated with DPD for 24 h were fixed with 4% paraformaldehyde for 20 min, washed three times with PBS for 5 min each time, and blocked by applying PBS containing 0.5% Triton and 1% bovine serum albumin (BSA) for 2 h. The cells were then incubated with primary antibody on a shaker at 4 °C overnight. After three washes with PBS, Fluor488 (P0176) and Fluor647 (A0473) fluorescently labeled secondary antibodies were added and incubated for 1 h with protection from light and washed three times with PBS. Finally, fluorescence was observed under a confocal microscope. Image analysis was performed using ImageJ Fiji (NIH, Bethesda, USA).

ROS assay

U87MG and LN229MG cell densities reached approximately 60–70% when DPD was added for 48 h. Dichlorodihydrofluorescein diacetate (DCFH-DA, Beyotime, Shanghai, China, S0033S) was diluted with serum-free cell culture solution (1:1000) to make a final concentration of 10 μmol/L. The cell culture medium was removed, 0.5 mL of the diluted DCFH-DA was added, and the cells were incubated for 20 min at 37 °C in a cell culture chamber. The cells were washed three times with serum-free cell culture solution, incubated for 20 min, treated with anti-quenching sealer containing 4′,6-diamidino-2-phenylindole (DAPI, P0131) and observed directly under a laser confocal microscope. If using flow cytometry to observe the ROS level, cells were collected, treated with 0.5 mL of diluted DCFH-DA, incubated in a cell culture incubator at 37 °C for 20 min, washed, and analyzed using a FACS Calibur flow cytometer (BD. C6 Plus, USA). Data were analyzed using FlowJo software.

JC-1 assay

After U87MG and LN229MG cells had been cultured with DPD in 12-well plates for 48 h, 0.5 mL of cell culture medium and 0.5 mL of JC-1 (Beyotime, Shanghai, China, C2006) staining working solution were added, mixed well, and then incubated at 37 °C for 20 min. Carbonyl cyanide 3-chlorophenylhydrazone (CCCP) was used as a positive control to reduce MMP. CCCP was added to the cell culture solution at a ratio of 1:1000, diluted to 10 μM, and the cells were incubated for 20 min. At the end of the incubation, the supernatant was aspirated, the cells washed twice with JC-1 staining buffer (1X), cell culture medium (1 mL) was added, and a laser confocal microscope was used for observation. MMP levels were subsequently measured by flow cytometry. Cells were collected, resuspended in cell culture medium (0.5 mL), treated with JC-1 staining working solution (0.5 mL), inverted, mixed well, and then incubated at 37 °C for 20 min. After washing, the cells were analyzed using a FACS Calibur flow cytometer (BD. C6 Plus, USA).

Determination of ATP concentration

U87MG and LN229MG cells in 6-well culture plates were treated with DPD for 24 h. The culture medium was aspirated and lysis buffer (200 μL) was added to each well to lyse the cells. After lysis, the cells were centrifuged at 12,000 *g* for 5 min at 4 °C and the supernatant taken for subsequent analysis. At the same time, an ATP standard sample and working solution were prepared (Beyotime, Shanghai, China, S0027). ATP assay working solution (100 μL) was added to the assay wells and left at room temperature for 3–5 min. Sample or standard (20 μL) was quickly added into the assay wells and the ATP

concentration was determined using a multifunctional enzyme marker (Tecan A-5082, Made in Austria).

Tetramethylrhodamine methyl ester (TMRM) assay

U87MG and LN229MG cells were treated with DPD for 48 h. TMRM staining solution (100 nM, 1 mL, Invitrogen, USA, I34361) was added and incubated at 37 °C for 30 min. The cells were then washed twice with PBS, treated with PBS (1 mL) and an anti-quenching blocking solution containing DAPI. The cells were then directly observed under a laser confocal microscope.

In vivo experiments

Approximately 5×10^6 U87MG cells were injected subcutaneously into the dorsal position of 5-week-old BALB/c nude mice to establish a subcutaneous tumor model. The volumes of the transplanted tumors were measured and calculated every three days: tumor volume (mm^3) = $a \times b^2 \times 1/2$ (a = long diameter of the tumor; b = short diameter of the tumor); the weights of the nude mice were also recorded. The mice were euthanized after 15 d of treatment. Tumors were removed from the mice, fixed with 4% paraformaldehyde, and stained immunohistochemically.

Immunohistochemistry

Formaldehyde-fixed tumor tissues were embedded, sectioned, deparaffinized, hydrated, and then high-pressure repaired for antigen treatment. The slides were blocked with BSA for 30 min, and then incubated overnight at 4 °C with primary antibody. The secondary antibody was then added and incubated at room temperature for 1 h. The nuclei were stained with 3,3'-Diaminobenzidine(DAB) and hematoxylin re-staining, and all the staining results were analyzed using ImageJ Fiji software. Ki67 protein expression was assessed by calculating the percentage of positive cells and applying the positive area ratio to evaluate the expression of other proteins. Tumor tissues were dehydrated, embedded, sectioned, stained with dihydroethidium (DHE), and the nuclei were stained. A fluorescence microscope (Nikon, Japan) was used to observe and capture images, and the red fluorescence in cells was analyzed using ImageJ Fiji software to determine the levels of cellular ROS.

Hematoxylin & eosin (HE) staining

Fresh tissues were fixed in 4% paraformaldehyde for more than 24 h, then subjected to dehydration, embedding, sectioning, tissue baking, deparaffinization, and gradient hydration. Hematoxylin was used to stain the nuclei, and eosin to stain the cytoplasm, followed by dehydration, sealing microscopy and image acquisition (Nikon, Japan).

Statistical analysis

Data in all experiments are presented as the mean ± SD. Statistical analysis was conducted with GraphPad Prism 8.0 software, using two-tailed Student's test or one-way/two-way analysis of variance (ANOVA). P-value < 0.05 was considered statistically significant ($^{*}P < 0.05$; $^{**}P < 0.01$; $^{***}P < 0.001$;$^{****}P < 0.0001$; $\#P < 0.05$; $\#\#P < 0.01$; $\#\#\#P < 0.001$; $\#\#\#\#P < 0.0001$; NS stands for no significant change).

Results

DPD inhibits the proliferation of glioblastoma cell lines

The results from the CCK8 assay indicated that DPD (chemical structure in Fig. 1A) inhibited U87MG, LN229MG, and U251MG cell viability (Fig. 1B). Cell viability at 48 h gradually decreased as the dose was increased. As shown in Fig. 1C and D, the colony formation assay results showed that DPD significantly inhibited the proliferation of GBM cells in a dose-dependent manner. In the Annexin V-FITC/PI assay, there was no noticeable increase in the proportion of double-positive cells after drug treatment (Fig. 1E and F). There were also no significant changes in the expression levels of caspase-3 or cleaved PARP, markers of apoptosis (Fig. 1G). The above results suggest that DPD can inhibit proliferation of GBM cells, but apoptosis is not the main inhibitory pathway.

DPD modulates autophagy in glioma cells

After finding that DPD did not significantly affect apoptosis in GBM cells, we examined type 2 programmed death (autophagy). To confirm a correlation between DPD concentration and autophagy, the expression levels of LC3-II and p62 were determined after incubating U87MG and LN229MG cells with DPD at concentrations of 0, 7.5, 15, and 30 μM for 24 h. The results showed that DPD increased the expression of LC3-II and p62 in a dose-dependent manner (Fig. 2A). When GBM cells were treated with 30 μM DPD for 0, 6, 12, and 24 h, a time-dependent increase in expression of LC3-II and p62 was also noted (Fig. 2B), suggesting that DPD is a phytochemical with autophagy-regulating activity. The effect of DPD on autophagy was then further explored by observing and analyzing the formation of GFP-LC3-labeled autophagosomes. The findings showed that in normal control cells, the fluorescent signals of GFP-tagged LC3 were few and scattered, while a significant increase in GFP-LC3 spots was seen in two DPD-treated GBM cell lines (Fig. 2C and D). 3-Methyladenine (3-MA) is an inhibitor of phosphoinositide 3-kinase (PI3K) and inhibits autophagy upstream of the autophagosome formation stage; bafilomycin A1 (BafA1) is an inhibitor of the late stage of autophagy, blocking the fusion of autophagosomes with lysosomes and inhibiting lysosomal acidification and

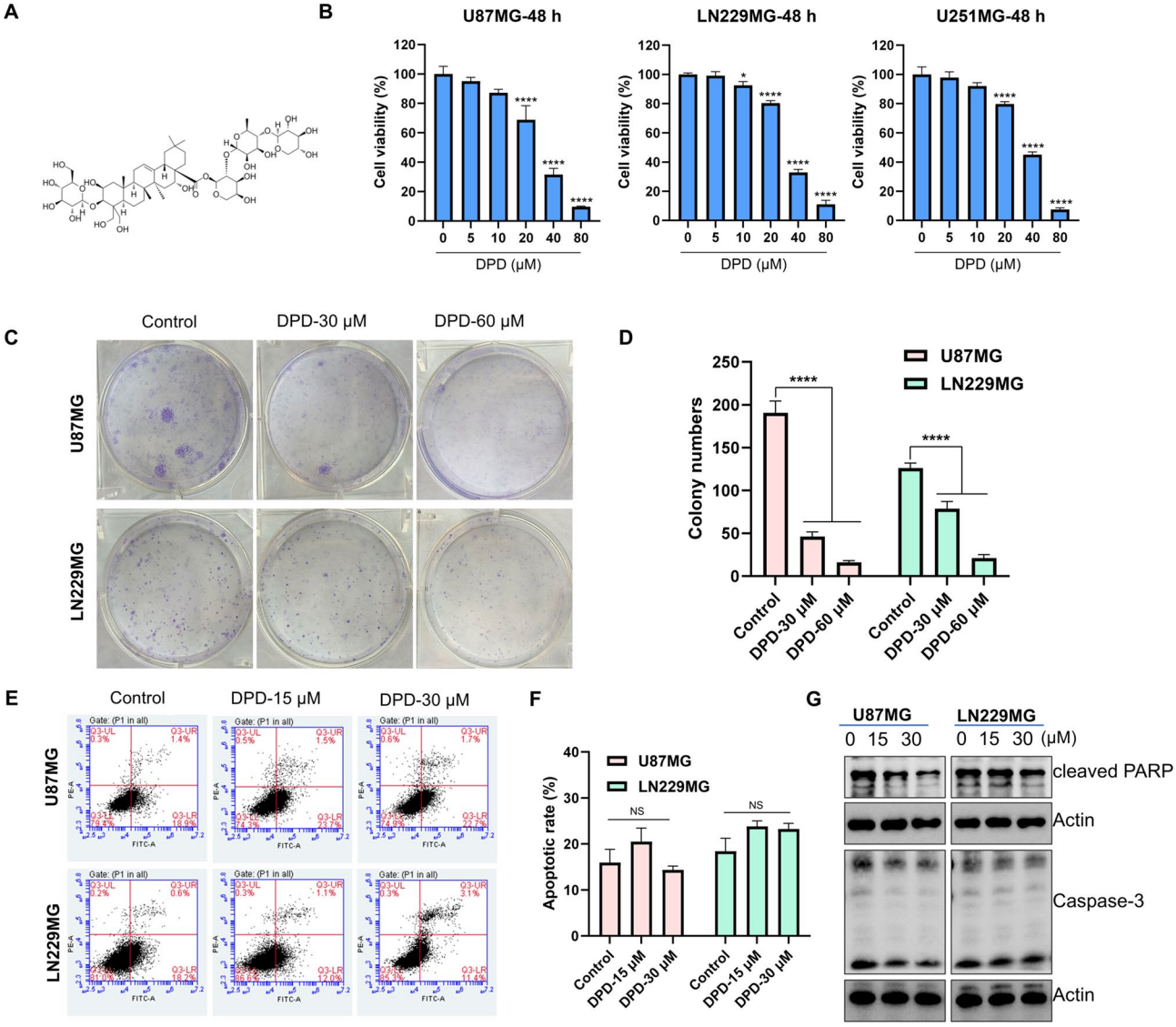

Fig. 1 DPD inhibits GBM cell proliferation through a non-apoptotic pathway. **A**) DPD chemical structure. **B**) Three cell lines, U87MG, LN229MG, and U251MG, were treated with a specified concentration of DPD for 48 h. Cell viability was measured by CCK8 assay. **C**, **D**) U87MG and LN229MG cells were treated with the indicated concentrations of DPD for 10 d. A colony formation assay was used to measure the proliferative capacity of the cells (**C**), and the number of colonies (≥ 50 cells) was counted using ImageJ Fiji software (**D**). **E**, **F**) GBM cells were treated with the indicated concentrations of DPD for 48 h. After staining with Annexin V-FITC/PI, the cells were analyzed by flow cytometry (**E**), and the apoptosis rate was calculated (**F**). **G**) Expression levels of caspase-3 and cleaved PARP in U87MG and LN229MG cells after 48 h treatment with DPD. The experimental data are expressed as mean ± SD (NS no significant change; $^{*}P < 0.05$; $^{**}P < 0.01$; $^{***}P < 0.001$; $^{****}P < 0.0001$, compared with the control group)

protein degradation. CCK8 assay of 3-MA + DPD-treated GBM cells showed a relative decrease in cell death, while a significant increase in cell death was observed after treatment with BafA1 + DPD, compared with DPD alone (Fig. 2E); crystal violet staining gave similar results (Fig. 2F). These results suggest that DPD-modulated autophagy in GBM cells might be the main pathway mediating DPD inhibition of GBM cell proliferation.

DPD blocks autophagy in the late stage

As a receptor for ubiquitinated protein aggregates, p62 is degraded by protein hydrolases in autophagy lysosomes during the late phase of autophagy. Since p62 levels were not significantly reduced after DPD treatment of GBM cells, we hypothesized that DPD might block the process of autophagy-lysosome formation. To assess the autophagy process, we used Ad-mCherry-GFP-LC3B, an adenovirus that enables expression of the mCherry-GFP-LC3B fusion protein to generate infected cells that express red and green fluorescence for the detection of autophagy.

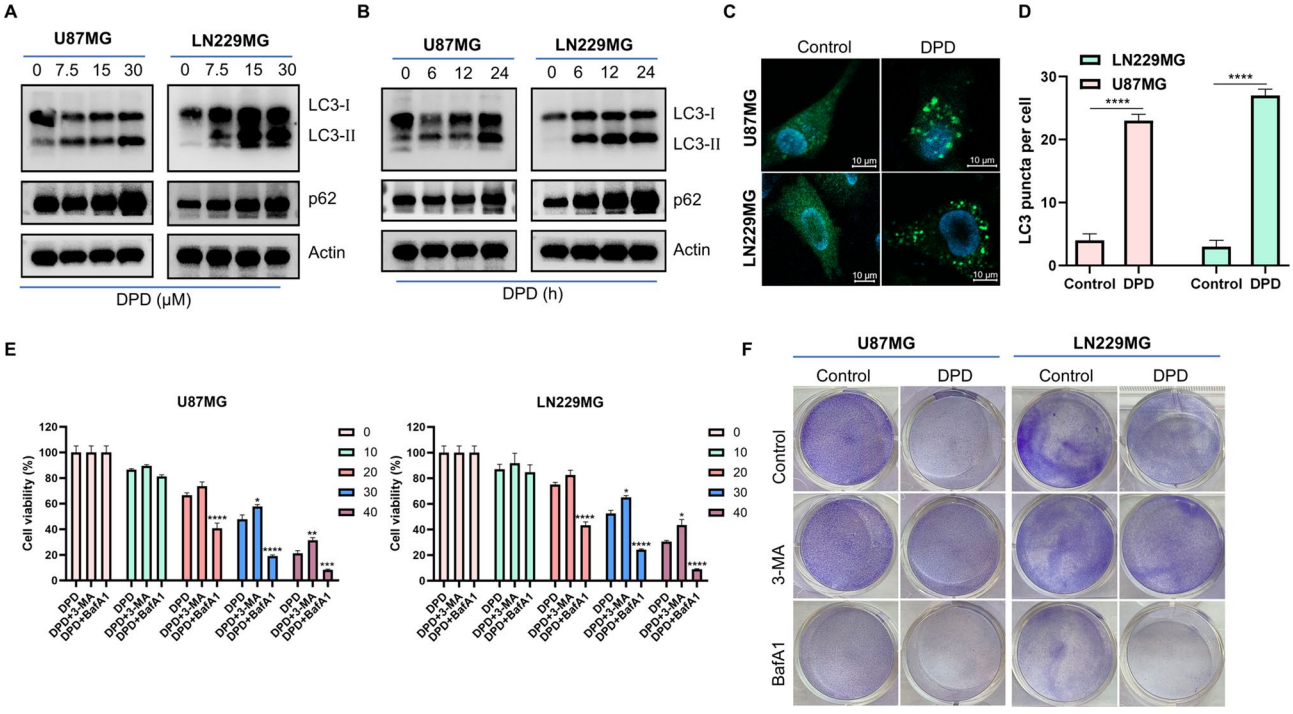

Fig. 2 DPD inhibits GBM cell proliferation by regulating GBM cell autophagy **A**) Level of LC3-II and p62 expression in U87MG and LN229MG cells after 24 h incubation with DPD at concentrations ranging from 0 to 30 μM. **B**) Level of LC3-II and p62 expression after 0, 6, 12, and 24 h incubation of DPD with U87MG and LN229MG cells. **C**) U87MG and LN229MG cells expressing GFP-LC3 fluorescence were treated with 0 or 30 μM DPD for 48 h. The cells were visualized by confocal microscopy (scale bar = 10 μm). **D**) GFP-LC3 spots were manually counted in 10 GBM cells in the experiment, and the average number was calculated to plot a histogram. **E**) After treatment with 3-MA or BafA1, GBM cells were then treated with the indicated concentrations of DPD for 48 h. CCK8 was used to determine cell viability. **F**) Crystal violet staining images of GBM cells treated with 3-MA or BafA1 combined with 30 μM DPD for 48 h. Experimental data are expressed as mean ± SD (*$P < 0.05$; ***$P < 0.001$; ****$P < 0.0001$, compared with the control group)

The acidic environment in the lysosome during fusion of autophagic vesicles with lysosomes leads to quenching of the GFP fluorescence, but GFP fluorescence was not significantly reduced after DPD action on GBM cells (Fig. 3A and B). This suggests that integration of autophagosomes and lysosomes is suppressed, and the autophagic lysosomal process is blocked. To further clarify the inhibitory effect of DPD on late autophagy, we stained GBM cells expressing GFP-LC3 with the red fluorescent dye LysoTracker Red, thus exploring whether DPD affects autophagosome-lysosome fusion. Confocal imaging showed that in both GBM cell lines, the GFP-LC3 spots resulting from treatment with DPD did not co-localize with LysoTracker Red, similar to cells treated with BafA1 (Fig. 3C and D). Western blot showed no decrease in p62 levels occurring after treatment of GBM cells with both DPD and BafA1 (Fig. 3E). These experimental results indicated that DPD mediated incomplete autophagy in GBM cells.

Transcriptomic analysis of DPD-treated GBM cells

The Kyoto Encyclopedia of Genes and Genomes (KEGG) pathway annotated bar graphs of differentially expressed genes (Fig. 3F) show that after treatment of GBM cells with DPD, the differentially expressed genes were mainly enriched in the following areas: focal adhesion, regulation action, cytoskeleton, endocytosis, lysosome, phagosome, animal autophagy, PI3K-AKT signaling flux, pathway cytoskeleton, endocytosis, lysosome, phagolysosome, and pathway in cancer, among which endocytosis, lysosome, phagolysosome, animal autophagy, PI3K-AKT signaling flux, and pathway in cancer are all related to autophagy. A heat map (Fig. 3G) revealed more significant differences in autophagy-related genes such as SQSTM1 and BNIP3L. To further verify the occurrence of autophagy and identify the type of autophagy, we used TEM to observe the cellular structure after DPD treatment. After 48 h of drug treatment, a large number of damaged mitochondria (mitochondrial swelling, mitochondrial ridge breakage) were visible, and different stages of autophagy were apparent, as were a relatively large number of mitochondrial autophagosomes, and a relatively small number of autophagic lysosomal structures (Fig. 3H). Since BNIP3L is a critical gene that mediates mitophagy, DPD may modulate mitophagy through BNIP3L.

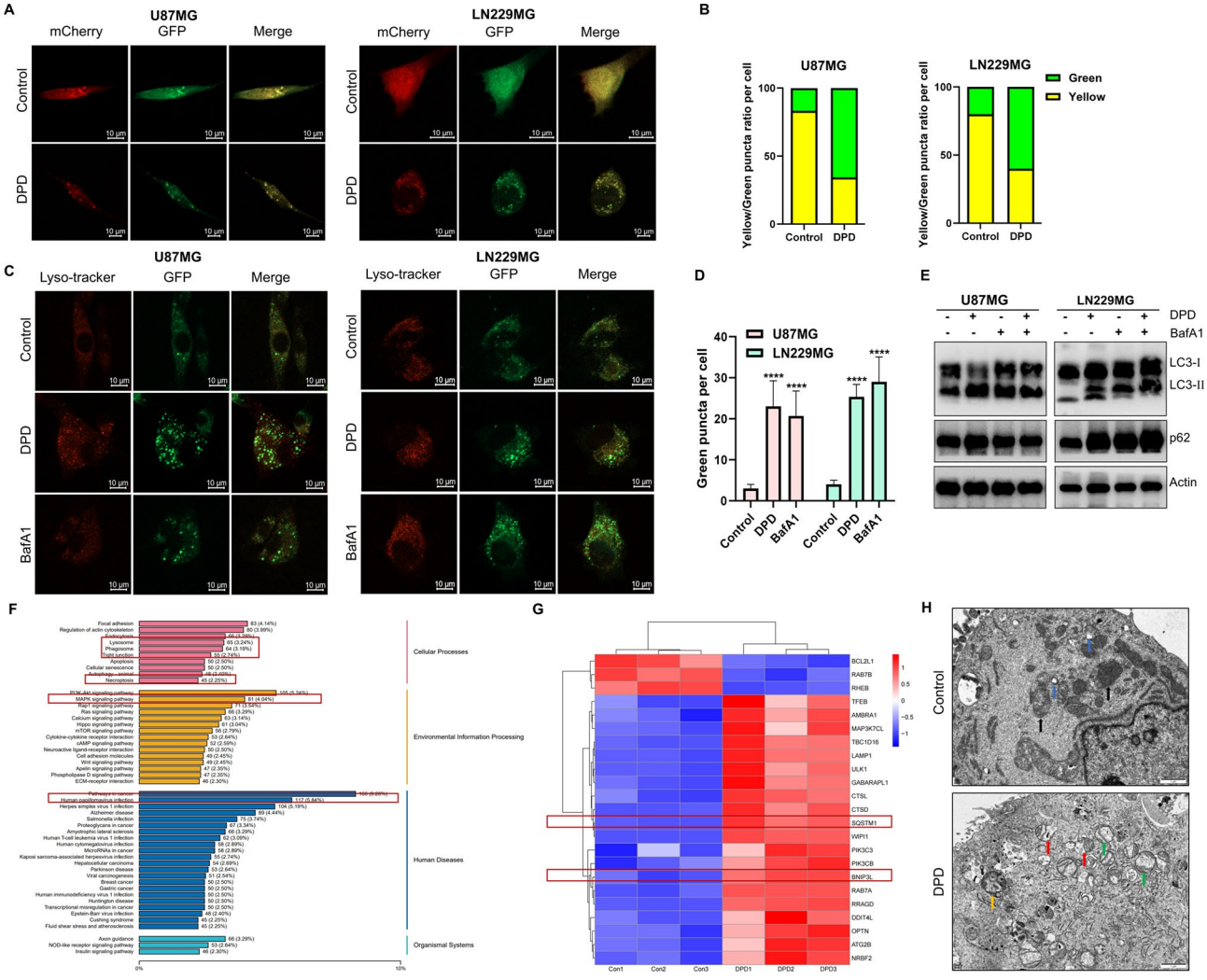

Fig. 3 DPD blocks autophagic flux in late phase; Transcriptomics and TEM imaging of DPD action on LN229MG **A**, **B**) U87MG and LN229MG cells expressing Ad-mCherry-GFP-LC3B were treated with 0 or 30 μM DPD for 48 h. Images were taken under a confocal microscope (**A**), scale bar = 10 μm. Ten cells were counted manually, and the average was taken to analyze the ratio of yellow-green spots (**B**). **C**, **D**) U87MG and LN229MG cells expressing GFP-LC3 were treated with 0 or 30 μM DPD or 100 nM BafAl for 48 h, and then stained with LysoTracker Red and imaged under a confocal microscope (**C**). The green spots in each cell were quantified by manually counting ten cells and taking the average value (**D**), scale bar = 10 μm. E) p62 protein levels after DPD or/and BafA1 treatment of GBM cells. **F**) An annotated map of the KEGG pathway differential genes after DPD treatment of LN229MG cells; those shown in red rectangular boxes are associated with cellular autophagy. **G**) Heatmap of selected genes with significant differences. **H**) Control mitochondria (black arrowheads) and lysosomes (blue arrowheads) in normal cells; a large number of damaged mitochondria (green arrowheads), mitochondrial autophagosomes (red arrowheads), and autophagic lysosomes (yellow arrowheads) were observed by TEM of drug-treated LN229MG cells after 48 h, scale bar = 1 μm

DPD causes mitochondrial damage and mitophagy

Mitochondria, responsible for energy metabolism in all eukaryotic cells, play a key role in maintaining cellular homeostasis. Excessive accumulation of ROS in cells and tissues leads to mitochondrial damage and permeability transition, resulting in mitochondrial depolarization, loss of membrane potential, and induction of mitophagy-associated protein activation. To determine the damage caused by DPD to mitochondria, we used confocal microscopy and flow cytometry to analyze ROS levels in GBM cells treated with DPD for 48 h. The results showed that DPD increased levels of ROS in GBM cells in a dose-dependent manner (Fig. 4A and C). To assess the effect of DPD on MMP, laser confocal microscopy and flow cytometry were used to detect fluorescence changes after JC-1 staining. It was found that the green fluorescence gradually increased after DPD treatment compared with control cells, indicating that MMP was decreased (Fig. 4D and F). To additionally verify the effect of 30 μM DPD on mitochondrial function, we analyzed ATP levels and showed that DPD decreased ATP levels in GBM cells (Fig. 4G). All of these results suggested that mitochondrial damage occurred in GBM cells after drug administration.

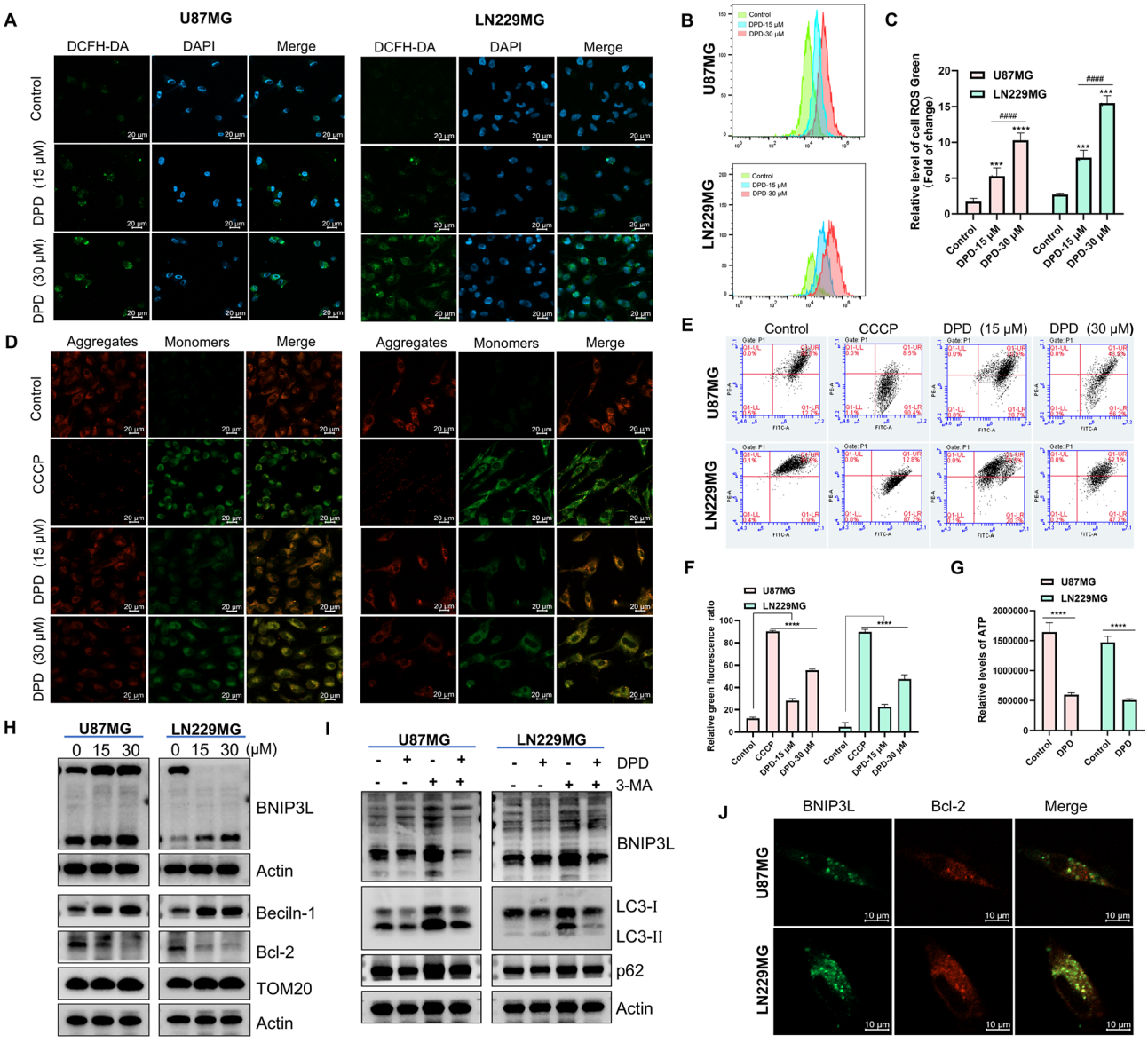

Fig. 4 DPD induction of mitophagy in GBM cells **A**, **C**) ROS (green fluorescence) expression after treatment of U87MG and LN229MG cells with 0, 15, and 30 μM DPD for 48 h. Confocal microscopy images (**A**), scale bar = 20 μm. Flow cytometry was used to assess ROS levels (**B**), and a histogram analysis was performed (**C**). **D**, **F**) Confocal microscope images of JC-1 staining in U87MG and LN229MG cells after treatment with 0, 15, and 30 μM DPD, and CCCP for 48 h (**D**), scale bar = 20 μm. Flow cytometry quantitative analysis (**E**) and histogram analysis (**F**). **G**) ATP concentrations after DPD treatment of GBM cells. **H**) BNIP3L, Bcl-2, Beclin-1, and TOM20 protein expression after DPD treatment of GBM cells. **I**) BNIP3L, LC3, and p62 protein expression after 3-MA and/or DPD treatment of GBM cells. J) Co-localized visualization of BNIP3L and Bcl-2 by laser confocal microscopy, scale bar = 10 μm. (*$P < 0.05$; ***$P < 0.001$; ****$P < 0.0001$, ####$P < 0.0001$, compared with control)

BNIP3L mediates mitophagy

We have found that cells with severe mitochondrial damage also contain damaged mitochondria in autophagosomes, and transcriptomic analysis showed that expression of the mitophagy-related gene BNIP3L was significantly altered. To verify that BNIP3L mediates mitophagy, western blotting was used to quantify related proteins. The results showed that when U87MG and LN229MG cells were treated with DPD, the levels of LC3-II, p62, BNIP3L and Beclin-1 proteins were increased, while the level of Bcl-2 protein was decreased. There was no significant change in TOM20 (a core component of the mitochondrial outer membrane transporter enzyme (TOM) complex that transports proteins synthesized in the cytoplasm to the interior of the mitochondria through three main steps of recognition, delivery, and transport, and is commonly used as a mitochondrial marker) (Fig. 4H). The above results suggest that increased expression of BNIP3L may have mediated mitophagy, while the unchanged levels of TOM20

suggest accumulation of damaged mitochondria, i.e., incomplete autophagy due to failed degradation of damaged mitochondria, which is consistent with our electron microscopy observations. Subsequently, a western blot of GBM cells treated with 3-MA and DPD together showed that autophagy-associated protein levels were not significantly elevated compared with normal control cells (Fig. 4I). This further verified that it was BNIP3L that mediated mitophagy and that the increased BNIP3L expression disrupted the Bcl-2-Beclin-1 complex pathway, releasing Beclin-1 and activating autophagy. Co-localization of BNIP3L and Bcl-2 was observed using immunofluorescence techniques (Fig. 4J), confirming that BNIP3L mediated mitophagy. When BNIP3L was knocked down and Bcl-2 was overexpressed in glioma cells, the suppressive effect of DPD on GBM cells was significantly weaker (Fig. 5A). The inhibitory effect of DPD on GBM cells was also significantly weakened by the addition of the mitophagy inhibitor Mdivi-1 (Fig. 5B). After knockdown of BNIP3L, autophagy was significantly reduced (Fig. 5C). Western blot showed that the levels of LC3-II and p62 were decreased considerably after knockdown of BNIP3L, and the level of p62 recovered to the that of the control group (Fig. 5D). The TMRM assay showed that the membrane potential level of GBM cells was reduced after knockdown of BNIP3L (Fig. 5E). After Bcl-2 overexpression, western blot showed that autophagy was inhibited (Fig. 5F). The data suggested that DPD induced mitophagy in GBM cells via BNIP3L-Bcl-2 signaling, leading to cell death.

In vivo experiments with DPD

U87MG cells were used to establish a subcutaneous tumor model in nude mice. There was a significant reduction in tumor volume throughout the drug treatment cycle. Silencing of BNIP3L or overexpression of Bcl-2 in conjunction with DPD treatment resulted in an increase of tumor volume compared with DPD-treatment alone (Fig. 6A and B). There was no appreciable difference in body weight of mice in the control group throughout the experimental period (Fig. 6C). Tumor immunohistochemistry showed that Ki67 levels were significantly decreased in the drug-treated group compared with the negative control group. Ki67 levels were increased after silencing of BNIP3L or overexpression of Bcl-2 in conjunction with drug-treatment compared with drug-treatment alone (Fig. 6D and E). DPD increased expression of LC3, p62, BNIP3L, and Beclin-1 and decreased Bcl-2 expression. Expression of LC3, p62, BNIP3L, and Beclin-1 was significantly reduced after silencing of BNIP3L, while overexpression of Bcl-2 resulted in significantly decreased expression of LC3, BNIP3L and Beclin-1 (Fig. 6F an 6G). The ROS levels were relatively increased in the TMZ- and DPD-treated groups, while ROS levels were decreased after silencing of BNIP3L or overexpression of Bcl-2 compared with drug-treatment alone (Fig. 6H and I). HE staining of histological sections from various organs after high-dose DPD-treatment in mice preliminarily confirmed the safety of DPD (Fig. 6J). The animal data are consistent with those from the cell experiments, indicating that DPD can induce incomplete autophagy of mitochondria and suppress proliferation of GBM cells in vivo and in vitro via BNIP3L.

Discussion

Autophagy is a cellular degradation and recycling process that plays a complex dual role in cancer as both a tumor suppressor and a tumor promoter [18]. Autophagy suppresses tumor initiation by providing anti-inflammatory functions, maintaining genomic stability, degrading potentially oncogenic proteins, participating in anti-cancer immune surveillance, maintaining normal metabolism for optimal bioenergetics, and contributing antiviral properties. However, autophagy can promote tumor progression and increase tumor metastasis in established tumors and advanced stages of tumor growth. Overall, the effects of autophagy seem to depend on the tumor stage, specific oncogenic mutations, and cellular environment. For this reason, more effective and specific targeted drugs that inhibit or activate autophagy must be applied in various tissues and at different stages of tumor development.

In the present study, DPD produced significant cytotoxic effects on different GBM cell lines at various concentrations. It was shown that DPD has the potential to be an anti-GBM drug. Subsequently, when analyzing the pathways modulated by DPD in GBM cells, it was found that DPD did not significantly induce apoptosis but strongly activated cellular autophagy. Under normal conditions, autophagy is a protective mechanism, but as a type 2 programmed death mode, it causes cell death when over-activated [19, 20]. Here, we found that DPD affects the binding of autophagosomes to lysosomes while activating autophagy, leading to blockage of late autophagic flow, which results in the accumulation of large numbers of autophagosomes in the cell, culminating in cell death in response to stress.

It has been found that different insults mediate the initiation of different types of autophagy. If damage to mitochondria occurs, the resulting autophagic process is called mitophagy [21]. In the present study, a large amount of mitochondrial damage was indeed observed by TEM, and autophagosomes contained damaged mitochondrial fragments. Therefore, we hypothesized that DPD may induce mitophagy. As organelles with significant involvement in cellular metabolism and signaling flux, mitochondria are particularly vulnerable to damage [22, 23], and their morphology and number are

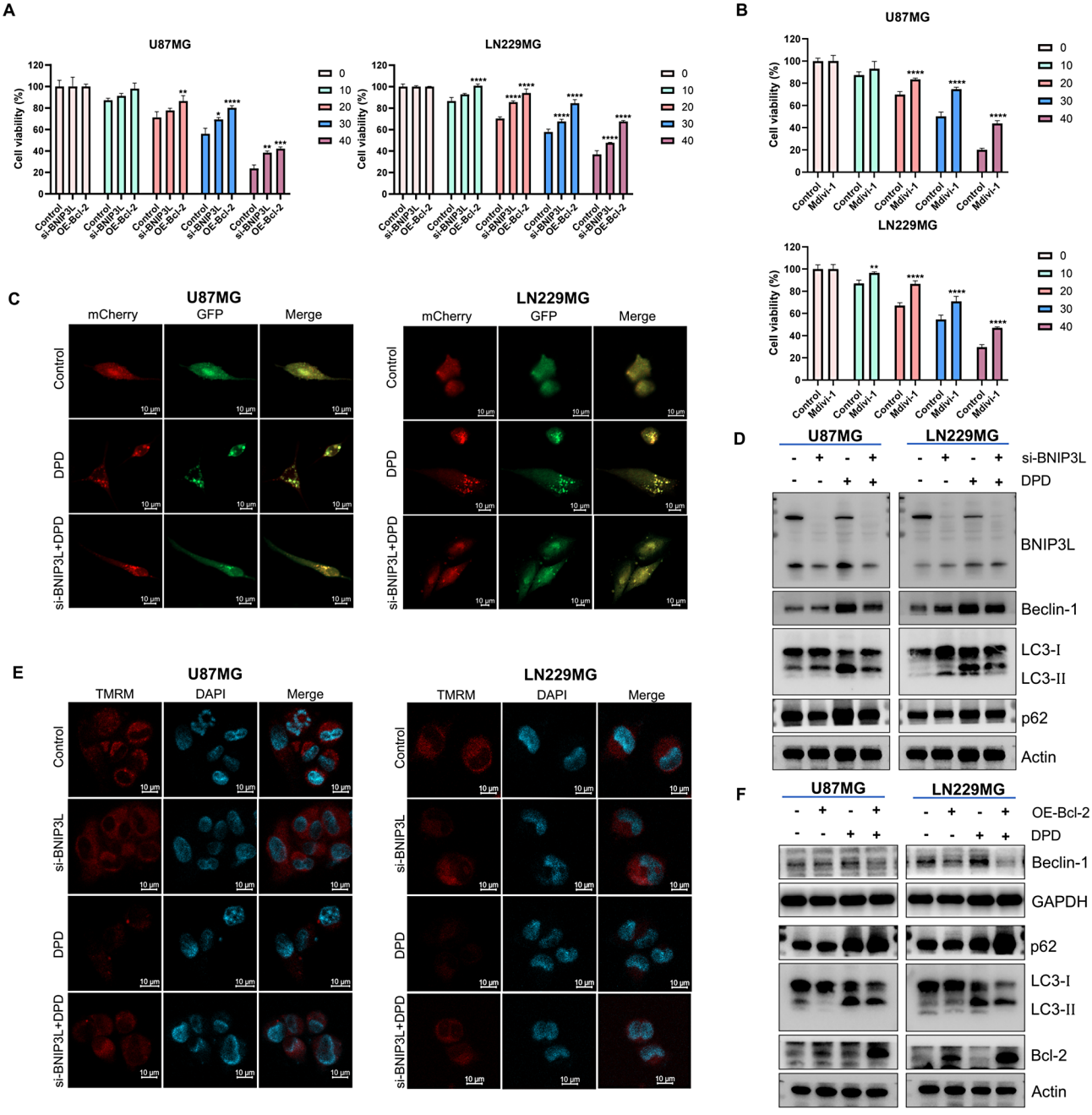

Fig. 5 BNIP3L induces mitophagy and causes cell death in GBM cells **A**) Cell viability of DPD-treated GBM cells after BNIP3L silencing and Bcl-2 overexpression. **B**) Cell viability of GBM cells after Mdivi-1 treatment. **C**) Effect of knockdown of BNIP3L on autophagy. **D**, **E**) BNIP3L, Beclin-1, LC3, and p62 expression levels (**D**) and cell membrane potential levels (**E**) of GBM cells after BNIP3L silencing and DPD treatment, scale bar = 10 μm. **F**) Beclin-1, p62, LC3, and Bcl-2 expression levels after transfection of GBM cells with Bcl-2 overexpression plasmid and treatment with DPD

dependent on physiological and pathological stimuli [24]. Mitophagy has been linked to cancer, neurodegenerative, and other diseases [25, 26]. Consequently, mitophagy is a therapeutic target in oncology [27].

We found significant changes in the autophagy-related gene BNIP3L during transcriptome data analysis. Following this observation, we analyzed mitochondrial damage and found that DPD decreased MMP and promoted ROS release. Western blot showed increases in BNIP3L and Beclin-1 levels and decreased levels of Bcl-2, and immunofluorescence showed co-localization of BNIP3L and Bcl-2. These results suggested that BNIP3L reduced MMP by competing with Beclin-1 for binding to Bcl-2, disrupting the Bcl-2-Beclin-1 complex [28, 29] and releasing Beclin-1 to activate autophagy. The reduced cytotoxicity of DPD after treatment with the autophagy

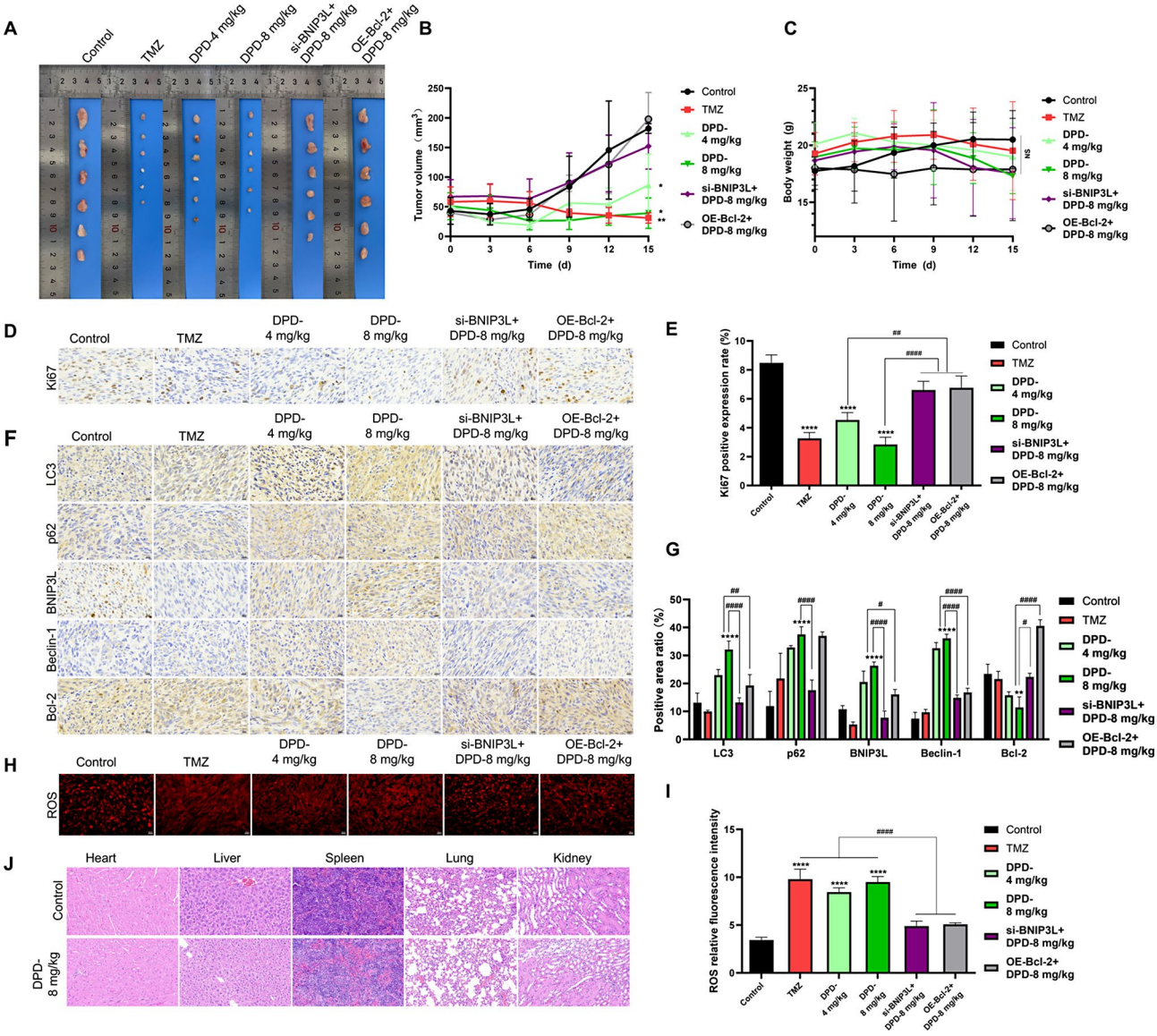

Fig. 6 Effects of DPD on GBM cells in vivo**A**) Images of tumor xenografts in each group. **B**) Average tumor volumes of model mice in each group during 15 d. **C**) Average body weight of model mice in each group over 15 d. **D**, **E**) Expression of Ki67 in different groups of tumor tissues (**D**) and histogram (**E**), scale bar = 20 μm. **F**, **G**) Expression of p62, LC3, BNIP3L, Beclin-1, and Bcl-2 in tumor tissues from different groups (**F**) and histogram (**G**), scale bar = 20 μm. **H**, **I**) Expression of ROS in tumor tissues from different groups after DHE staining (**H**) and histogram (**I**), scale bar = 20 μm. **J**) Histopathology of various organs from normal control and drug groups (HE x 40). (*$P < 0.05$; **$P < 0.01$; ***$P < 0.001$; ****$P < 0.0001$, #$P < 0.05$; ##$P < 0.01$; ###$P < 0.001$; ####$P < 0.0001$, compared with the control group)

inhibitors 3-MA and Mdivi-1 demonstrated that DPD inhibits GBM proliferation by targeting the mitophagy pathway. Silencing of BNIP3L reduced the cytotoxicity of DPD towards GBM and decreased the level of autophagy, suggesting that DPD indeed induces mitophagy in GBM cells via BNIP3L. It has been reported in the literature that BNIP3L has different roles in mitophagy, and in the case of acute brain injury, BNIP3L protects the brain from damage [30]. In contrast, a recent paper reported that BNIP3L overactivation is deleterious, that knockdown of BNIP3L inhibits mitophagy overactivation and rescues lifespan in Fbxl4$^{-/-}$ mice [31], and that elevating BNIP3L induces mitochondrial autophagic overactivation. This finding adds to the understanding of mitophagy regulation, which is echoed in the results from this study.

It was determined that mitophagy occurred following DPD treatment of GBM cells, and BNIP3L was experimentally verified as a receptor and activator of mitophagy. Autophagic flow was blocked in the late phase, suggesting that mitophagy was incomplete. TEM showed that mitochondria were damaged and there was an accumulation of damaged mitochondria. Most

autophagic vesicles were not fused with lysosomes and cleared, implying that DPD induced mitophagy through BNIP3L as a receptor, which eventually blocked autophagic flow in the late autophagic phase, resulting in failed recycling of damaged mitochondria and subsequent cell death. These findings are significant because it has been reported that cancer cells are dependent on mitochondria to meet cellular energy requirements and there are few studies on the effect of increased BNIP3L expression on glioblastoma cell survival [11, 32].

As mentioned earlier, BNIP3L has a dual role in cancer, inhibiting and promoting tumor development [33]. Here, we found that DPD-induced mitophagy caused late autophagic flow obstruction, resulting in intracellular accumulation of many damaged mitochondria. In contrast, silencing of BNIP3L alleviated the late autophagic flow obstruction, suggesting that DPD not only activates mitophagy but also promotes death of GBM cells through accumulation of damaged mitochondria in a dual manner. The same BNIP3L-mediated mitophagy has very different effects on disease, so we cannot analyze the phenomenon of mitophagy in isolation. Rather, the whole process of mitophagy, with or without over-activation, impaired clearance of damaged mitochondria, and impaired mitochondrial accumulation, recycling, and reuse must be evaluated. Incomplete autophagy differs from ordinary autophagy in that it predominantly promotes cell death, thus incomplete autophagy is a viable target for anti-tumor therapy [34].

DPD blocks late autophagic flow properties, making it very clinically promising, and it may potentiate the cytotoxic effects of chloroquine and TMZ. TMZ-induced protective autophagy is a key factor mediating GBM chemoresistance, so DPD has promise for reversal of TMZ resistance [35]. Glioma stem cells (GSC) are the drivers of metastasis and tumor recurrence, and DPD can inhibit the self-renewal and stemness of GSC by induction of incomplete autophagy [36]. DPD is a promising antitumor drug but still faces many challenges because its safety and toxicity have not been thoroughly studied. Although immunohistochemistry of various organs from drug-treated mice did not show pathological damage, further studies are required, for example, on gastrointestinal tract kinetic function, animal behavior, different drug dosing regimens, and different routes of administration.

There are some shortcomings and limitations in this study. A limited number of GBM cell lines and animal models were used, the number of experimental animals and the duration of experimental drug administration were also limited, and determination of the optimal therapeutic dose of DPD and potential off-target effects and toxicity were also lacking. DPD induces a blockage of autophagic flux in the late phase, but the underlying mechanisms still require further in-depth studies. A broader understanding of the pathways modulated by DPD, and mechanisms other than mitochondrial autophagic flux, is desirable. The initial experimental design was aimed at determination of the anti-GMB effect of DPD, so there was no consideration of TMZ and DPD co-administration for in vitro or in vivo experiments. In the future we can consider the effects of TMZ/DPD combination, and even DPD-treatment of TMZ-resistant GBM cell lines. Moreover, because of the relatively large molecular weight of DPD, permeation of the blood-brain barrier is limited, and a mouse intracranial in situ tumor model was not established. In future experiments, we will conduct an in-depth study, and may design and fabricate a new type of nano-drug delivery system for delivery of DPD, alone or in combination with other drugs. We would like to establish an intracranial in situ GBM tumor model and evaluate the anticancer efficacy of DPD and other drugs, such as TMZ, individually or synergistically.

In summary, we found that DPD induced incomplete mitophagy in GBM cells through BNIP3L, and also inhibited tumor cell proliferation by impairing fusion of autophagosomes and lysosomes, blocking late autophagic flow, and aggravating mitochondrial damage and accumulation. Therefore, DPD is a potential anti-GBM drug that targets mitophagy. This study provides a new theoretical basis for DPD-targeted autophagy in the treatment of glioblastoma.

Abbreviations

BafA1	Bafilomycin A1
BSA	Bovine serum albumin
CCK8	Cell counting kit-8
DPD	Deapioplatycodin D
DHE	Dihydroethidium
GBM	Glioblastoma
JC	1-JC-1 mitochondrial membrane potential detection kit
KEGG	Kyoto Encyclopedia of Genes and Genomes
MMP	Mitochondrial membrane potential
PBS	Phosphate-buffered saline
ROS	Reactive oxygen species
TMRM	Tetramethylrhodamine methyl ester
TEM	Transmission electron microscopy
TMZ	Temozolomide
3	MA-3-methyladenine

Acknowledgements
Not applicable.

Author contributions
Yu Sun: Writing-original draft, Methodology, Data curation. Guangze Zhu: Validation, Investigation, Conceptualization. Renshuang Zhao: Investigation, Methodology. Yaru Li: Data curation. Hongyang Li: Formal analysis, Software. Yunyun Liu: Investigation. Ningyi Jin: Supervision. Xiao Li: Resources, Funding acquisition.Yiquan Li: Writing-review & editing, Methodology, Funding acquisition, Project administration. Tiemei Liu: Writing review & editing, Supervision, Funding acquisition. All authors have reviewed the manuscript and approved the final version of this paper.

Funding
This work was supported by the Youth Outstanding Subject Backbone Training Program of Changchun University of Chinese Medicine (Grant No.

202318), the Science and Technology Research Project of Jilin Provincial Department of Education (Grant No. JJKH20241039KJ), and the Jilin Province Traditional Chinese Medicine Science and Technology Project (No. 2024254).

Data availability
No datasets were generated or analysed during the current study.

Declarations

Ethics approval and consent to participate
All animal experimental protocols followed the guidelines for ethical review of laboratory animal welfare and were approved by the Animal Care and Use Committee of Changchun University of Chinese Medicine.

Consent for publication
Not applicable.

Competing interests
The authors declare no competing interests.

Author details
[1]Department of Blood Transfusion, China-Japan, Union Hospital of Jilin University, Changchun 130033, P.R. China
[2]Department of Neurology, Jilin Central Hospital, Jilin 132011, P.R. China
[3]Academician Workstation of Jilin Province, Changchun University of Chinese Medicine, Changchun 130117, P.R. China
[4]Medical College, Yanbian University, Yanji 133002, P.R. China
[5]Changchun Veterinary Research Institute, Chinese Academy of Agricultural Sciences, Changchun 130122, P.R. China
[6]Jingyue Economic & Technological Development Zone, No. 1035, Boshuo road, Changchun, Jilin, P. R. China

Received: 6 July 2024 / Accepted: 6 January 2025
Published online: 13 January 2025

References

1. Thakur A, Faujdar C, Sharma R, Sharma S, Malik B, Nepali K, et al. Glioblastoma: current status, emerging targets, and recent advances. J Med Chem. 2022;65:8596–685.
2. Tan AC, Ashley DM, López GY, Malinzak M, Friedman HS, Khasraw M. Management of glioblastoma: state of the art and future directions. CA Cancer J Clin. 2020;70:299–312.
3. Li H-Y, Feng Y-H, Lin C-L, Hsu T-I. Mitochondrial mechanisms in Temozolomide Resistance: unraveling the Complex interplay and therapeutic strategies in Glioblastoma. Mitochondrion. 2024;75:101836.
4. Mizushima N, Komatsu M. Autophagy: renovation of cells and tissues. Cell. 2011;147:728–41.
5. Debnath J, Gammoh N, Ryan KM. Autophagy and autophagy-related pathways in cancer. Nat Rev Mol Cell Biol. 2023;1–16.
6. Lee S, Son J-Y, Lee J, Cheong H. Unraveling the intricacies of Autophagy and Mitophagy: implications in Cancer Biology. Cells. 2023;12:2742.
7. Dp P, Pp P, Cs B, Kk M, Bp SP. B, The emerging, multifaceted role of mitophagy in cancer and cancer therapeutics. Seminars in cancer biology [Internet]. 2020 2024(14);66. Available from: https://pubmed.ncbi.nlm.nih.gov/31351198/
8. Fei P, Wang W, Kim S, Wang S, Burns TF, Sax JK, et al. Bnip3L is induced by p53 under hypoxia, and its knockdown promotes tumor growth. Cancer Cell. 2004;6:597–609.
9. Gallegos ZR, Taus P, Gibbs ZA, McGlynn K, Gomez NC, Davis I, et al. EWSR1-FLI1 activation of the Cancer/Testis Antigen FATE1 promotes ewing sarcoma survival. Mol Cell Biol. 2019;39:e00138–19.
10. Meyer N, Zielke S, Michaelis JB, Linder B, Warnsmann V, Rakel S, et al. AT 101 induces early mitochondrial dysfunction and HMOX1 (heme oxygenase 1) to trigger mitophagic cell death in glioma cells. Autophagy. 2018;14:1693–709.
11. Jung J, Zhang Y, Celiku O, Zhang W, Song H, Williams BJ, et al. Mitochondrial NIX promotes Tumor Survival in the hypoxic niche of Glioblastoma. Cancer Res. 2019;79:5218–32.
12. Zhang L, Wang Y, Yang D, Zhang C, Zhang N, Li M, et al. Platycodon grandiflorus – an Ethnopharmacological, phytochemical and pharmacological review. J Ethnopharmacol. 2015;164:147–61.
13. Qin H, Du X, Zhang Y, Wang R, Platycodin D. A triterpenoid saponin from Platycodon grandiflorum, induces G2/M arrest and apoptosis in human hepatoma HepG2 cells by modulating the PI3K/Akt pathway. Tumour Biol. 2014;35:1267–74.
14. Yu JS, Kim AK. Platycodin D induces reactive oxygen species-mediated apoptosis signal-regulating kinase 1 activation and endoplasmic reticulum stress response in human breast cancer cells. J Med Food. 2012;15:691–9.
15. Zhou R, Lu Z, Liu K, Guo J, Liu J, Zhou Y, et al. Platycodin D induces tumor growth arrest by activating FOXO3a expression in prostate cancer in vitro and in vivo. Curr Cancer Drug Targets. 2015;14:860–71.
16. Ouyang J, Li H, Wu G, Hei B, Liu R. Platycodin D inhibits glioblastoma cell proliferation, migration, and invasion by regulating DEPDC1B-mediated epithelial-to-mesenchymal transition. Eur J Pharmacol. 2023;958:176074.
17. Li H, Ouyang J, Liu R. Platycodin D suppresses proliferation, migration, and invasion of human glioblastoma cells through regulation of Skp2. Eur J Pharmacol. 2023;948:175697.
18. Galluzzi L, Pietrocola F, Pedro JMB-S, Amaravadi RK, Baehrecke EH, Cecconi F et al. Autophagy in malignant transformation and cancer progression. The EMBO Journal [Internet]. 2015, 2024(28); Available from: https://www.embopress.org/doi/https://doi.org/10.15252/embj.201490784
19. Liu S, Yao S, Yang H, Liu S, Wang Y, Autophagy. Regulator of cell death. Cell Death Dis. 2023;14:1–17.
20. Denton D, Kumar S. Autophagy-dependent cell death. Cell Death Differ. 2019;26:605–16.
21. Ashrafi G, Schwarz TL. The pathways of mitophagy for quality control and clearance of mitochondria. Cell Death Differ. 2013;20:31–42.
22. Amorim JA, Coppotelli G, Rolo AP, Palmeira CM, Ross JM, Sinclair DA. Mitochondrial and metabolic dysfunction in ageing and age-related diseases. Nat Rev Endocrinol. 2022;18:243–58.
23. K Y MO. M S, N M, K O. Molecular mechanisms and physiological functions of mitophagy. The EMBO journal [Internet]. 2021, 2024(14);40. Available from: https://pubmed.ncbi.nlm.nih.gov/33438778/
24. Picard M, Taivassalo T, Gouspillou G, Hepple RT. Mitochondria: isolation, structure and function. J Physiol. 2011;589:4413–21.
25. Wang S, Long H, Hou L, Feng B, Ma Z, Wu Y, et al. The mitophagy pathway and its implications in human diseases. Signal Transduct Target Ther. 2023;8:304.
26. Picca A, Faitg J, Auwerx J, Ferrucci L, D'Amico D. Mitophagy in human health, ageing and disease. Nat Metab. 2023;5:2047–61.
27. Poole LP, Macleod KF. Mitophagy in tumorigenesis and metastasis. Cell Mol Life Sci. 2021;78:3817–51.
28. Zhang J, Ney PA. ROLE OF BNIP3 AND NIX IN CELL DEATH, AUTOPHAGY, AND MITOPHAGY. Cell Death Differ. 2009;16:939–46.
29. Mazure NM, Pouysségur J. Atypical BH3-domains of BNIP3 and BNIP3L lead to autophagy in hypoxia. Autophagy. 2009;5:868–9.
30. Ma J, Ni H, Rui Q, Liu H, Jiang F, Gao R, et al. Potential roles of NIX/BNIP3L pathway in Rat Traumatic Brain Injury. Cell Transpl. 2019;28:585–95.
31. Cao Y, Zheng J, Wan H, Sun Y, Fu S, Liu S, et al. A mitochondrial SCF-FBXL4 ubiquitin E3 ligase complex degrades BNIP3 and NIX to restrain mitophagy and prevent mitochondrial disease. EMBO J. 2023;42:e113033.
32. Bellot G, Garcia-Medina R, Gounon P, Chiche J, Roux D, Pouysségur J, et al. Hypoxia-induced autophagy is mediated through hypoxia-inducible factor induction of BNIP3 and BNIP3L via their BH3 domains. Mol Cell Biol. 2009;29:2570–81.
33. Li Y, Zheng W, Lu Y, Zheng Y, Pan L, Wu X, et al. BNIP3L/NIX-mediated mitophagy: molecular mechanisms and implications for human disease. Cell Death Dis. 2021;13:14.
34. Zhang Q, Cao S, Qiu F, Kang N. Incomplete autophagy: trouble is a friend. Med Res Rev. 2022;42:1545–87.
35. Ou M, Cho H-Y, Fu J, Thein TZ, Wang W, Swenson SD, et al. Inhibition of autophagy and induction of glioblastoma cell death by NEO214, a perillyl alcohol-rolipram conjugate. Autophagy. 2023;19:3169–88.
36. You F, Li C, Zhang S, Zhang Q, Hu Z, Wang Y, et al. Sitagliptin inhibits the survival, stemness and autophagy of glioma cells, and enhances temozolomide cytotoxicity. Biomed Pharmacother. 2023;162:114555.

Publisher's note